ELSEVIER

Catalysis Today 58 (2000) 89–102

CATALYSIS TODAY

www.elsevier.com/locate/cattod

Photoreactions of small molecules at the surface of alkali metal halides

Vladimir Ryabchuk

Institute of Physics, SPbSU, Ulianovskaia 1, St Petersburg 198904, Russia

Abstract

The photostimulated reactions of small molecules, i.e., O_2 photoadsorption and photodesorption, H_2 and CO photooxidation, and CO_2 photodecomposition on alkali halides (alkali halides) surface are discussed in this work. Most of 19 alkali halides show the activity in the reactions mentioned above. Three spectral regions of alkali halides stimulation by light are distinguished in relation to kinetics of oxygen photoadsorption and reactivity of adsorbed oxygen species. They are in correspondence with: (i) bulk exciton absorption bands; (ii) extrinsic and intrinsic bulk and surface absorption bands and (iii) color centers absorption bands. In the latter case the activity of alkali halides arises after pre-excitation in exciton bands, which leads to sensitization of alkali halides to visible light. The H_2 and CO photooxidation on alkali halides is two-step photoprocess involving some excited states of adsorbed oxygen. The latter is quenching by gaseous oxygen as it is shown for hydrogen oxidation over KBr. The photodecomposition of carbon dioxide is treated as CO_2 dissociative adsorption with CO evolution into the gas phase.

Keywords: Alkali halides; Photoadsorption; Photooxidation; Carbon dioxide photodecomposition; Heterogeneous photocatalysis

1. Introduction

Today heterogeneous photocatalysis is known mainly as photocatalysis on semiconductors [1–3]. Moreover, several essential properties of titanium dioxide (TiO_2) make it most promising for practical usage and the most popular photocatalyst. However, solids other than oxides, alkali halides in particular, demonstrate a variety of surface photostimulated processes such as photostimulated adsorption (photoadsorption), desorption (photodesorption), and photostimulated chemical transformation of molecules at a gas/solid interface. Interestingly, some processes that we put refer to photostimulated heterogeneous ones (e.g., the photodissociation of adsorbed molecules) were described first for alkali halides and alkali earth fluoride vacuum deposited films with adsorbed I_2, Br_2 and NO_2 by De Boer [4] and Terenin [5] in early 1930s.

There were two motives to renew the studies of photoreactions of small molecules on alkali halides two decades ago. The first one appeared due to the demonstration of photolysis of water adsorbed on dispersed KCl, KBr and NaCl along with 15 wide band-gap oxides [6]. The second motive is more abstract. The wide band-gap alkali halides have a relatively simple structure, and serve as model subjects in the theoretical studies of crystalline, defect and electronic properties of solids since 1920. The alkali halides were also used as model solids in the early studies of light absorption, photostimulated defect formation (photocoloration) and photoconductivity [7]. In contrast to the wide band-gap oxides, the so-called decay of excitons on the Frenkel pairs in alkali halides regular lattice along with free carriers generation occur under photoexcitation in fundamental and exciton absorption bands [8,9]. As a result, additional and even extraordinary surface centers (active sites) can be created at the sur-

0920-5861/00/$ – see front matter
PII: S0920-5861(00)00244-3

face of alkali halides by light in comparison to those, created via carriers trapping by pre-existing defects.

For alkali halides, gas adsorption effect on photocoloration, color bleaching, photo and thermally stimulated luminescence, etc. was reported in many early works. This indirectly proves alkali halides surfaces to be active in heterogeneous photoreactions. We are not able to comment all these works here. We also do not refer to high energy radiation induced processes at the gas/alkali halides interfaces. The latter, in contrast to photostimulated processes, are studied rather intensively [10].

Therefore, we focus on the photostimulated reactions of small molecules on alkali halides in order to enlarge our knowledge on photostimulated processes in the gas/solid heterogeneous systems, and to compare alkali halides with the wide band-gap oxides. The recent interest in photostimulated reactions on alkali halides is caused by the problems of natural photocatalysis [11] and heterogeneous photochemistry of the atmosphere [12–15].

2. Experimental

Experiments were done in a high vacuum set-up (residual pressure ca. 10^{-7} Pa) equipped with oil-free pumping systems. Pirani-type manometers were used to control total gas pressure in the reaction cell. Reactors volumes involving quartz cells were 30–70 cm^3. Gas composition in the reaction cell was analyzed and TPD spectra of adsorbed molecules were obtained using mass-spectrometers (MX-7301, APDM-1).

Powdered samples in the flat 4–5 mm path length quartz cell (illuminated cells area 3.5–6 cm^2) were irradiated most by a 120 W high pressure mercury lamp (DRK-120, MELZ). Photon flow at wavelength below 260 nm was about 1×10^{15} photons $cm^{-2}\,s^{-1}$. For KBr excitation in the first exciton band were used hydrogen hole-cathode 30 W lamp (DDS-30) or quartz low pressure mercury lamp (DRT-230, $\lambda=185$ nm) placed at 5 mm from the front cell window, thermostated with air flow. Experiments with vacuum deposited KBr and KI films (thickness ~0.03–0.05 cm) were done in quartz cells with a path length 2 cm and a front area 25–50 cm^2. Glass cut-off filters or monochromator MDR-2 (LOMO) were used to select the excitation regions.

The diffuse reflectance spectra ($BaSO_4$ as standard) of UV-colored samples were recorded in situ with spectrophotometer Specord M-40 (Karl Zeiss, Jena). In this case a whole high vacuum set-up was moved from the position of sample pre-treatment and irradiation to that of spectra recording.

Commercial superfine and fine grade purity alkali halides powders were used. To remove the adsorbed gases and surface contamination, powdered alkali halides were alternatively heated on vacuuming or in oxygen ($p_0=100$ Pa) for several tens of hours at 700–750 K. After heating their $S_{BET}\leq1\ m^2\,g^{-1}$. Samples were considered to be pure, when their surface evolved 80–90% of photoadsorbed oxygen on heating up to baking temperature and when results, obtained on irradiation on vacuuming or in oxygen were reproducible. The stochiometric consumption of H_2 and O_2 on hydrogen photooxidation (see below) was additional criterion for the alkali halides surface purity.

Along with the powdered samples, we have studied thin films of KBr and KI, deposited on the inner side of the back (with respect to light source) cell window in vacuum. In these cases only super fine grade purity samples of KBr and KI (total contents of metals $\sim10^{-3}$%) pre-treated as described above were used for deposition. The slices of KBr monocrystal, purified by the 60th-fold zone melting (Institute of Solid State Physics, Tartu, Estonia), with a total content of any impurities ≤1 ppm were also used for the thin films deposition. The average crystallites size in deposited KBr films is estimated as 1×10^{-3} cm by microscope. The details of experimental techniques are described in [16].

3. Results and discussions

3.1. Photostimulated adsorption of oxygen

Photoadsorption of O_2 and CO_2 was observed on all alkali halides tested, whereas on NaF, KF, CsF and CsCl relatively weak photoadsorption of H_2 and CO only was noticed [16,17]. The photoadsorption of Br_2 was also observed for KBr [18]. The photoadsorption kinetics, i.e., O_2 and CO_2 pressure versus irradiation time in closed reactor are irreversible at room temperature, and has no measurable latent time ($t_l<1$ s), rate is decreasing with time for all alkali halides. Initial

steady-state O_2 photoadsorption rate (A) versus gas pressure p for KBr and KI [18,19] can be expressed as

$$A = \frac{dp}{dt} = \frac{kKp}{(1 + Kp)} \quad (1)$$

where k is the apparent rate constant, and K differs from the equilibrium adsorption constant for the Langmuir–Hinshelwood kinetics of photocatalytic reaction. Here K is treated as ratio $K=k_a/k_d$, between a bimolecular constant of interaction of a gaseous molecule with a photoinduced surface active center (active site) k_a and the first-order decay constant, k_d for the active center. (For further discussion of this approach see the first work of Rapoport et al. [20], and the recent work of Emeline et al. [21].) Estimated values of parameter $\tau_d=1/k_d$, i.e., the life time of the photoinduced active center for O_2 photoadsorption on KBr and KI ranges within 10^{-1}–10^{-4} s [18,19]. On the other hand, on the alkali halides we see oxygen post-adsorption, i.e., the adsorption of O_2 molecules in the dark on preliminary irradiated by the UV-light in vacuum. The values of the so-called post-adsorption coefficient $\Omega=N_a/N_{ph}$, where N_a is the number of molecules adsorbed after irradiation for a given pre-illumination time period in vacuum, and N_{ph} is the number of photoadsorbed O_2 molecules for the same exposure time, do not exceed 0.1. For most alkali halides thermal desorption spectra show several poor resolved peaks at 350–750 K [16].

The tentatively estimated oxygen photoadsorption red limits λ_r (or corresponding threshold energies of photons E_r) on the annealed alkali halide powders lay far beyond the alkali halides bulk exciton bands (E_{ex}) (Table 1) and fundamental adsorption edges E_g [22]. Regarding the high content of impurities in powdered alkali halides tested, one may suppose the photoexcitation of impurities and associated intrinsic lattice defects to be responsible for the oxygen pho-

Table 1
Relative activities of alkali halides in photostimulated adsorption (PSA), photooxidation (PSO) and photodecomposition (PSDC)

Alkali halide	Excitation band, E_{ex} (eV)	PSA O_2 red limit		PSA		PSO		PSDC
		E_r (eV)	λ_r (nm)	$A(O_2)$	$A(CO_2)$	$V(H_2)$	$V(CO)$	$\Delta p(CO_2)$
LiF	12.9	3.9	320	0.2	0.6	0.01	0.01	0.03
NaF	10.7	3.9	320	0.4	0.4	0.05	0.03	0.5
KF	9.88	3.5	350	1.6	0.7	0.9	1.0	1.7
RbF	9.54	4.4	280	2.0	2.0	0.25	1.0	1.3
CsF	9.27	2.9	430	2.5	–[a]	0.6	1.5	0.8
LiCl	8.67	5.3	230	0.4	0.01	0.01	0.03	0.01
NaCl	7.96	4.4	280	0.3	0.6	0.05	0.05	0.5
KCl	7.79	4.4	280	0.2	0.01	0.01	0.2	0.03
RbCl	7.54	3.9	320	0.15	0.01	0.1	0.15	0.5
CsCl	7.85	5.3	230	0.6	0.5	0.1	0.5	1.9
LiBr	7.23	3.2	390	0.7	0.01	0.01	0.05	0.01
NaBr	6.71	3.5	350	0.15	0.25	0.1	0.01	0.9
KBr	6.71	3.9	320	1.0[b]	1.0[b]	1.0[b]	1.0[b]	1.0[b]
RbBr	6.64	4.4	280	1.5	–[a]	1.5	0.8	–[a]
CsBr	6.83	4.4	280	1.0	1.4	0.3	0.2	–[a]
NaI	5.61	5.3	230	0.3	2.3	0.01[c]	0.01[c]	0.8
KI	5.88	5.3	230	0.2	1.6	0.01	0.02	1.3
RbI	5.73	5.3	230	0.8	0.15	0.01	0.01	1.6
CsI	–[a]	4.4	280	0.4	1.6	0.05	0.05	0.5

[a] No data.

[b] The alkali halides activities are presented in relative units. KBr activities $A(O_2)=1.1\,mPa\,s^{-1}$, $A(CO_2)=0.075\,mPa\,s^{-1}$, $V(H_2)=2.4\,mPa\,s^{-1}$, $V(CO)=0.23\,mPa\,s^{-1}$ and $\Delta p=0.12$ Pa are accepted as units for the reactions. The initial gas pressure is $p_0 = 0.5$ Pa for any reaction. The amount of preliminary photoadsorbed oxygen in the case of the photooxidation of H_2 and CO is $\Delta p(O_2)=0.04$ Pa. The irradiation of the samples is carried out with DRK-120 mercury lamp.

[c] The initial flow rates of H_2 and CO under illumination of iodides with photoadsorbed oxygen is detectable, but unlike the rest low active alkali halides, the effect ended soon.

toadsorption in the near λ_r red limits spectral region at any rate. However, except for the observed "blue shift" of the red oxygen photoadsorption limit from $\lambda_r \approx 320$ nm for powders to $\lambda_r \approx 250$ nm for vacuum deposited KBr films, the other O_2 photoadsorption and photoreactions features studied are the same. It will be emphasized that KBr films prepared from the zone melted monocrystal slices, satisfy the surface purity criterion (see Section 2) after the first vacuum deposition without any thermal pre-treatment in oxygen. Moreover, with monocrystal slices initial oxygen photoadsorption rates at $Kp \gg 1$ (Eq. (1)), normalized to the unit area of the cell window, are even higher than with powdered KBr samples. Initial oxygen photoadsorption rate for powdered KBr, averaged over 50 measurements for five different sample loading and pre-treatment is $A=(1.1\pm0.1)\,\mathrm{mPa\,s^{-1}}$ or $(3\pm0.3)10^{12}\,\mathrm{mol\,s^{-1}\,cm^{-2}}$ [17]. The overall content of impurities in the films, prepared from the KBr crystal slices does not exceed 10^7 per crystallite particle. This amount is equal to the total number of intrinsic surface defects (low-coordinated ions associated with kinks, terraces, edges, corners, fragments of high index facets) at the surface of vacuum deposited KBr particles since the density of such defects can exceed $10^{12}\,\mathrm{cm^{-2}}$ for alkali halides [23]. Hence most likely the surface bound excitons associated with intrinsic surface defects, participate in the photoadsorption of O_2 on alkali halides. This type of solid excitation in heterogeneous photoreactions has been well proved for alkali-earth metal oxides [24].

Initial photoadsorption rate values, A, obtained are presented in Table 1. Though photoadsorption activities A were measured at the same gas pressure, same light intensity and after the same sample pre-treatment they are not proper ones to compare the photoadsorption activity of different alkali halides [17]. Nevertheless, note that averaged O_2 photoadsorption activity increases monotonously with metal atomic number increasing for fluorides, and chlorides show the lowest average activity. Alkali halides activities in different reactions are compared in some more details elsewhere [25,26]. In our experiments, solely alkali metal iodides were excited in their bulk exciton absorption bands (Table 1), since the highest photon energy of the actinic light was close to 6.2 eV ($\lambda \geq 200$ nm). The kinetics of photoadsorption of O_2 and CO_2 on iodides differs from that for the rest alkali halides [16]. In turn, KBr behavior under irradiation in the first exciton band ($\lambda_{max}=187$ nm at $T=300$ K) is similar to that of iodides [19]. The amount of oxygen, photoadsorbed at sufficiently long exposure time, was more than by one order of magnitude higher than that on photoadsorption induced in extrinsic absorption bands. From the kinetics of the "exciton" O_2 photoadsorption, which follows the Solonitzyn's photoadsorption kinetics for uniformly irradiated surface [27], the low limits of the so-called ultimate photoadsorption capacity for KBr and KI vacuum deposited films are estimated as $\theta_\infty \sim 5\times10^{12}\,\mathrm{mol\,cm^{-2}}$ [16]. The lower limits of θ_∞ obtained for KBr and KI are ca. 10-fold higher than that for TiO_2 [28] and close to θ_∞ for $MgAl_2O_4$ [29] and TiO_2 supported on SiO_2 [30]. The TPD spectra of oxygen photoadsorbed on KBr under irradiation in the exciton and extrinsic absorption bands, are also different (Fig. 1, curves 1 and 2, respectively). So one may assume that different oxygen species are generated at the KBr surface, when O_2 photoadsorption, depending on either bulk excitons or extrinsic and/or intrinsic surface defects are excited by actinic light. Among the oxygen-containing defects anions O_2^-, O^-, O^{2-} have been registered in the alkali

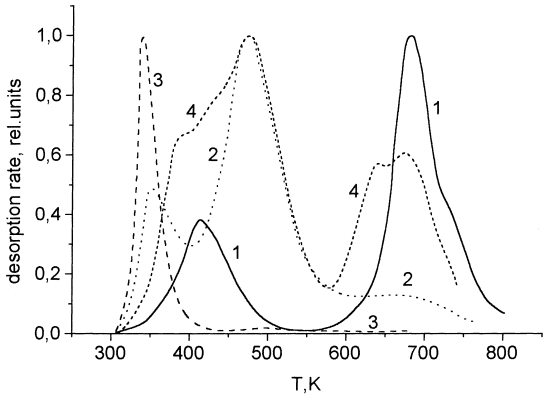

Fig. 1. TPD spectra of oxygen ($m/e=32$) for the vacuum deposited KBr film: after O_2 photoadsorption under illumination with $\lambda=185$ nm (the number of adsorbed molecules $N_a=5.6\times10^{15}$ mol) — (curve 1); after in spectral region $200<\lambda<250$ nm ($N_a=5.6\times10^{14}$ mol) — (curve 2); after O_2 photoadsorption in spectral region $500<\lambda<750$ nm ($N_a=3.4\times10^{14}$ mol) with UV pre-excitation ($\lambda=185$ nm, pre-exposure time $t=15$ min in vacuo) — (curve 3); after CO_2 photoadsorption ($200<\lambda<250$ nm, exposure time 30 min, $N_a=8.8\times10^{14}$ mol) — (curve 4). The rate of linear heating during TPD spectra recording is $\beta=0.24\,\mathrm{K\,s^{-1}}$.

halides lattice with UV spectroscopy, luminescence and ESR techniques [31]. However, no ESR signals corresponding to the photoadsorbed oxygen were detected for KBr, KI, KCl and CsCl powders under experimental conditions quite similar to ours [32].

3.2. Photostimulated desorption of oxygen

The TPD spectra of oxygen after photoadsorption of O_2 stimulated in both exciton and extrinsic absorption bands in parallel look like a slightly transformed curve 1 (Fig. 1), obtained after λ=185 nm irradiation. Such a "non-additivity" of the TPD spectra results from the photodesorption of photoadsorbed oxygen (at $\lambda \geq 200$ nm) KBr irradiation of an exciton band (λ=185 nm) [33]. A typical photodesorption curve, i.e., O_2 photodesorption rate (dN_{mol}/dt) versus irradiation time for the KBr film may be approximated by the first-order decay kinetics: $dN_{mol}/dt = C_1 \exp(-t/\tau_1) + C_2 \exp(-t/\tau_2)$. Constants C_1, τ_1 and C_2, τ_2 may be attributed to the photodesorption of two oxygen species, corresponding to two main peaks in the TPD spectrum (Fig. 1, curve 2). Typically, desorption rates are $dN_{mol}/dt \leq 1 \times 10^{13}$ mol s^{-1} cm^{-2}, while parameters τ_1 and τ_2 range within few seconds. A half of preliminary photoadsorbed oxygen can be removed from the surface via photodesorption. Peaks with T_{max}=360 K and with T_{max}=470 K (Fig. 1, curve 2) disappear, while peak with T_{max}=410 K arises (not shown), most probably due to the re-adsorption of oxygen, evolving into a gas phase on photodesorption. So, the evolution of the TPD spectrum from curve 2 to curve 1 (Fig. 1) partly takes place during the photodesorption of oxygen.

Photodesorption rate decreases with decreasing temperature by exponential law: $\ln(dN_{mol}/dt)_{max} \sim 1/T$. Activation energy estimate $E_a = (0.38 \pm 0.1)$ eV. No photodesorption of O_2 is observed at T<180 K. The temperature range of O_2 photodesorption coincides with the temperature range (T_d>175 K) of delocalization of both self-trapped holes and self-trapped excitons for KBr [34]. Self-trapped holes in the alkali halides lattice have configuration of an X_2^- halogen ion occupying two anion vacancy sites [36]. Self-trapped exciton is a pair of bound electron and self-trapped hole. They both move in the alkali halides lattice due to delocalization and re-trapping. Hence, oxygen photodesorption may be presented as

$$O_2^-(\text{ads}) + e^0(\text{or } h^+) \rightarrow O_2(\text{gas}) + e^-(\text{or } O_2(\text{gas})) \quad (2)$$

Here O_2^-(ads) is a photoadsorbed oxygen species; e^0, e^-, h^+ notify excitons, electrons and holes, respectively. Oxygen ions react with excitons as with *F* centers in the alkali halides [36]. Note the mechanism of oxygen photodesorption with primary solid photoexcitation (Eq. (2)) to differ from the alternative mechanism of photodesorption of molecules adsorbed at alkali halides surface with the direct photoexcitation of adsorbed species by actinic light [40].

3.3. Photo and thermally stimulated post-sorption of oxygen

As expected, the alkali iodides and KBr get color under illumination to bulk exciton bands. The color is provided by electron *F* centers forming in the alkali halides, since complementary hole (or halogen) *V*-color centers absorb UV-light. There are two basic mechanism of UV-coloration for the wide band-gap solids both valid for alkali halides: (i) through photo carriers trapping by pre-existing intrinsic and extrinsic defect, and exciton interaction with pre-existing defects and (ii) exciton decay into Frenkel pairs in the regular lattice yielding stable defects in the subsequent secondary reactions [8,9]. The photoexcitation of UV-colored alkali halides in their color centers bands causes partial bleaching, while baking to sufficiently high temperature yields complete decoloration.

On KI, RbI and KBr UV-irradiated in vacuum in their exciton bands O_2 (and CO_2) photoadsorption red limits shifts to 800–850 nm, which is far if compared with that for the annealed samples. By analogy to a post-sorption in the dark on preliminary irradiated solids in vacuum, this type of photoadsorption is named "photostimulated post-sorption" (PSPS) [37]. The PSPS O_2 rate dependence on the gas pressure on KBr and KI follows Eq. (1). The TPD spectra of oxygen after PSPS (Fig. 1, curve 3) partly coincide with that after the photoadsorption of O_2 (Fig. 1, curve 2). Photoadsorbed oxygen species (peak at T=350 K, curve 3) can be removed from the surface via photodesorption on KBr irradiation in exciton band. Thus, the PSPS of O_2 is rather similar to the oxygen pho-

toadsorption, stimulated in extrinsic absorption region ($200 \leq \lambda \leq 250$ nm for KBr vacuum deposited films). The *F* centers are responsible for light absorption during the PSPS of O_2. This assumption is confirmed by a linear dependence of initial PSPS rate on the concentration of UV-induced *F* centers observed, as well as by spectral and temperature dependencies of PSPS quantum yield on KBr and KI. The spectral dependence of O_2 PSPS on KBr is presented (Fig. 2, circle 1). The quantum yield of photoadsorption is defined as: $\Phi = (dN_{mol}/dt)/(dN_{ph}/dt)$, where dN_{mol}/dt is the photoadsorption rate (mol s^{-1}), and dN_{ph}/dt is the rate of photon absorption (photons s^{-1}). Quantum yield Φ is determined as the O_2 PSPS initial quantum yield, corresponding to initial (the highest) PSPS rate measured at $Kp \gg 1$, (Eq. (1)). Hence, it is equal to the quantum yield of active surface centers (sites) generation, since the photoadsorption dominates all other channels of active centers decay. The PSPS O_2 rate dependence on light intensity is linear, and thus Φ does not depend on the light intensity. Non-dimensional absorption coefficient $\Delta K(\lambda)$ (Fig. 2, curve 2) determines the rate of photons absorption by the UV-induced *F* centers placed in the colored layer of powder sample as $dN_{ph}/dt = \Delta K(\lambda)\Sigma I$, where Σ is the illuminated area of the cell front window, *I* the incident light intensity or photon flux (photons $cm^{-2}\,s^{-1}$). $\Delta K(\lambda)$ is equal to the difference between the coefficients of diffuse reflectance of powder sample before and after UV-irradiation $\Delta R(\lambda) = R_o(\lambda) - R(\lambda)$, and is similar in shape to the absorption spectrum of UV-induced color centers in powders [38]. Note, that this way of quantum yield calculation differs from that commonly accepted one, when total absorption, i.e., active and inactive (background) absorption is considered. However, in the latter case the spectral dependence of quantum yield does not consider the mechanism of photoadsorption or any other photocatalytic reaction. In particular, at a constant (spectral-independent) inactive background absorption, a dependence $\Phi(\lambda)$ is the more close in shape to $\Delta K(\lambda)$, the higher is the background adsorption [39]. It is clear from Fig. 2 that Φ of PSPS O_2, defined as mentioned above, does not depend on wavelength within the so-called *F* adsorption band (curve 2) of *F* center in KBr at $\lambda_{max} = 625$ nm. A simple approach, considering the spectral dependencies of quantum yields and reaction rates in the gas/solid and liquid/solid heterogeneous systems was recently proposed by Emeline et al. [39]. By this approach the PSPS O_2 active site (S^-) generation may be presented as the capture of photoelectrons e by some trap *S* at the surface: $S + e \rightarrow S^-$ with trapping rate constant k_{tr}. The initial photoadsorption rate at $Kp \gg 1$ (Eq. (1)), corresponding to starting concentration of surface traps S_0 is: $dS^-/dt = k_{tr}[S_0][n_s] \propto dN_{mol}/dt$, where the steady-state concentration of photoelectrons at the surface $[n_s]$ is determined by the solution of continuity equation

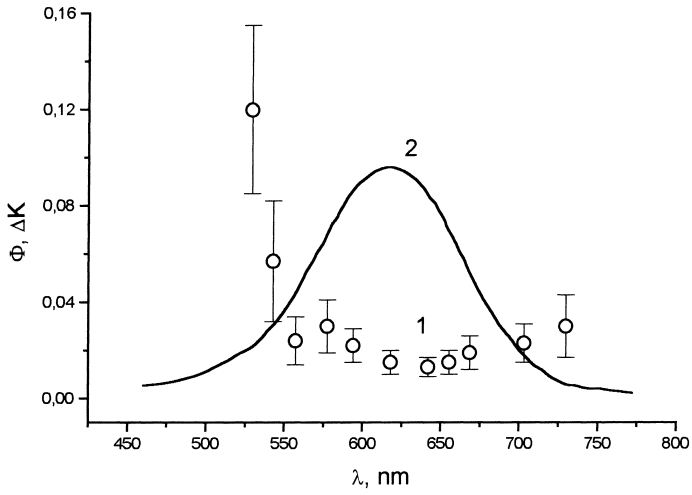

Fig. 2. Spectral dependence of quantum yield Φ of O_2 PSPS (curve 1) and spectral dependence of absorption coefficient ΔK (dot curve 2) for UV-colored KBr powder ($\lambda = 185$ nm, pre-exposure time $t = 15$ min in vacuo).

$$D\frac{\partial^2 n(x)}{\partial x^2} - \frac{n(x)}{\tau} + G(x) = 0 \quad (3)$$

Here $n(x)$ is the concentration of photoelectrons at point x in the crystallite particle bulk, D the diffusion coefficient of electrons, τ the life time of free photoelectrons with respect to several pathways of their trapping and recombination in solids. The first term in Eq. (3) describes electron diffusion, while the second term describes the pseudo first order decay of free electrons. A non-uniform function for photocarriers generation, $G(x)=\beta\alpha I\exp(-\alpha x)$, corresponding to the Lambert–Beer absorption law is chosen as the third-term. Here β is the so-called quantum yield of internal photoeffect or the probability of carrier generation up on photon absorption. Note that solely this generation function (or another space-dependent one) allows to consider the spectral dependencies for carriers concentrations as done in the early works on photoconductivity [41], photomagnetic field effect [42] and photolysis of AgBr [43]. In contrast, in the early works on photocatalysis, starting from the study of Wolkenstein and Karpenko [44] (see also [2,45–47]), the uniform function of generation $G=\alpha I$ is reasonably used, or the problem is reduced to case [44], ignoring any spectral dependence. General expression for $\Phi(\lambda)$, obtained for one-dimensional model, where a photocatalyst particle of size d is modeled by an infinitive plate of thickness d irradiating from both sides, is presented in [39]. Assuming the KBr crystallite size ($\sim 10^{-3}$ cm) and estimated absorption coefficient $\alpha=10^2\ \mathrm{cm}^{-1}$, corresponding to the F centers absorption, one may reduce the general expression for Φ to particular case

$$\Phi = \beta\, 2k_{\mathrm{tr}}\, S_0 \times f(D, d, L, s, \tau) \quad (4)$$

Note that there is no spectral-dependent adsorption coefficient $\alpha(\lambda)$ in Eq. (4). One may neglect spectral dependence Φ versus f, in turn, depending on diffusion coefficient D, and the diffusion length ($L^2=D\tau$) for carriers, and on the rate of surface recombination of carries s. So, Φ may depend on the wavelength of actinic light through β only. The spectral independence of Φ for PSPS O_2, i.e., plateau with the increasing Φ at the high energy edge of F band observed (Fig. 2) is in good agreement with the mechanism of photoionization of F centers [35,48].

Similarly, the O_2 adsorption in the dark on heating of preliminary UV-colored KBr (thermally stimulated post-sorption or TSPS), accompanying the thermal annealing of color has been observed in [37]. In this case the oxygen adsorption centers (active sites) are generated due to the thermal decay of UV-induced color centers in the alkali halides. Further details of the O_2 TSPS mechanism are presented elsewhere [27].

The nature of oxygen species, forming at the alkali halide surface on the photoadsorption of O_2 is still unclear, as well as the issue, why no hydrogen photoadsorption is detected on the KBr and iodides under illumination in exciton absorption bands. In the latter case, F centers and interstitial halogen atoms (through exciton decay into Frenkel pairs) are certainly created along with photoelectrons and photoholes (through several channels of exciton dissociation). Most likely, holes in the alkali halides take configuration of X_2^- molecular ion [35] in the regular alkali halides lattice (self-trapped hole) or near suitable defects (hole trapped by defect), and their chemical reactivity for some reasons is rather poor if compared to that of O^- trapped holes at oxides' surface [49].

In general, both photoadsorption and photodesorption of O_2 happen on the alkali halides. Three different spectral regions of alkali halides photoactivation are distinguished: (i) bulk exciton absorption bands; (ii) extrinsic bulk and surface bands, overlapping with surface intrinsic exciton-like bands and (iii) color centers bands, induced by the pre-illumination of alkali halides in the bulk exciton absorption bands. In case (iii) defects (color centers) photoinduction manifests itself as the spectral sensitization of alkali halides to visible light with respect to photoadsorption. The latter is rather common for the wide band-gap solids. Considering results, obtained for alkali halides, we find similar O_2 PSPS (and in some cases O_2 TSPS) for most of 21 wide band-gap oxides tested [26]. Relationship between photoadsorption and photostimulated defect formation, including PSPS and TSPS of both acceptor (O_2) and donor (H_2, CO) molecules was studied in more details with ZrO_2 [50], Sc_2O_3 [51] and $MgAl_2O_4$ [52].

3.4. Photooxidation of hydrogen and carbon monoxide

Photostimulated oxidation of H_2 and CO to H_2O and CO_2, respectively is observed on all alkali halides (except iodides) under illumination in $\lambda \geq 200$ nm spec-

tral region [17]. Besides, photooxidation of CH_4 to CO_2 and H_2O proceeds on KBr [53]. Photooxidation occurs when H_2 or CO and oxygen are in a gas phase, or when oxygen is pre-photoadsorbed. Neither noticeable adsorption of H_2, CO and O_2 in the dark nor H_2 and CO reaction with the photoadsorbed oxygen in the dark go on for most alkali halides. Thus, CO and H_2 photooxidation on alkali halides may be presented as two-step photoreaction, oxygen being adsorbed at the first step

$$O_2(\text{gas}) + h\nu + \text{alkali halides} \rightarrow O_2(\text{ads}) \quad (6a)$$

$$O_2(\text{ads}) + h\nu + H_2(\text{gas}) \text{ or } CO(\text{gas}) \rightarrow \text{products} \quad (6b)$$

H_2O molecules are detected at the surface only with the TPD in the case of H_2 photooxidation, whereas most CO_2 forms, when on photooxidation CO, evolves into a gas phase and then is readsorbed. With both reactions no preliminary photoadsorbed oxygen is detected on the surface after reactions end, provided that the initial H_2 and CO amounts exceed their stochiometric values. For most alkali halides [17], after 10–20 cycles of photoadsorption–photooxidation (Eqs. (6a) and (6b)) neither O_2 photoadsorption rate nor of H_2 and CO photooxidation rates decrease within a 10% measurement accuracy, despite reaction products accumulation at the surface of alkali halides. (Turnover numbers for the photooxidation of H_2 and CO were not determined. However, for CO_2 decomposition study (see below), the special quartz cell with KBr connected to the vacuum set-up was used to produce CO_2 by CO photooxidation.)

Table 1 shows the initial rates of H_2 and CO photooxidation (V), measured at the same content of preliminary photoadsorded oxygen (0.04 Pa) and at the same initial gas pressure (0.5 Pa). All alkali halide samples were irradiated by the full light of the same mercury lamp. Note, that some photooxidation red spectral limits are close to those for the photoadsorption of O_2. A number of linear correlations between O_2 photoadsorption initial rates and the rates of other photoreactions are revealed on alkali halides [25]. For example, correlation with coefficient r=0.90 and significance s>0.9999 between the initial O_2 photoadsorption rate and the rate of CO photooxidation for 19 alkali halides are presented in Fig. 3. So, most probably, the indirect activation of pre-adsorbed oxygen (Eq. (6b)) through the photoexcitation of solids takes place during photooxidation.

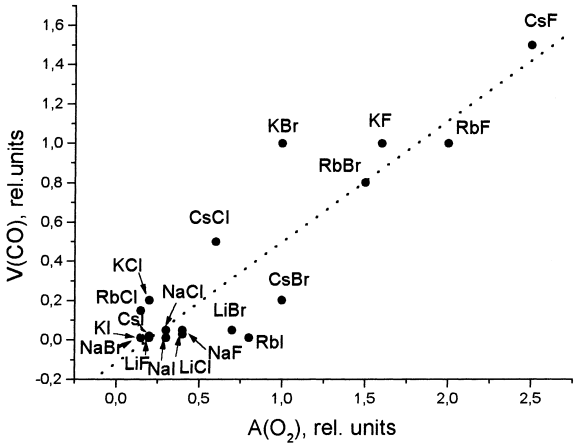

Fig. 3. Graphic representation of the correlation (r=0.90, s>0.9999) between O_2 PSA activity ($A(O_2)$) and the PSO of CO activity (V(CO)) for the alkali halides. (The activities are taken in units of KBr activities for the corresponding photostimulated reactions.)

The simplified mechanism has been proposed for the reaction second step (Eq. (6b)) regarding H_2 photooxidation on KBr [54]

1. $O_2(\text{ads}) + h\nu \rightarrow O_2^*(\text{ads})$ (k_a) (7a)
2. $O_2^*(\text{ads}) \rightarrow O_2(\text{ads})$ (k_d) (7b)
3. $O_2^*(\text{ads}) + O_2(\text{gas}) \rightarrow O_2(\text{ads}) + O_2(\text{gas})$ (k_q) (7c)
4. $O_2^*(\text{ads}) + H_2(\text{gas}) \rightarrow \text{products}$ (k_r) (7d)

At stage 1 some adsorbed oxygen species (O_2(ads)) are activated. O_2^* (ads) species actually are neither necessarily molecular nor neutral ones. The decay of active oxygen species is presented by the first-order process (stage 2). Stage 3 is the quenching of active oxygen species by gaseous oxygen. Both decay channels (stages 2 and 3) complete with the main reaction (stage 4).

Oxygen species, responsible to the first peak at T=360 K in the TPD spectrum (Fig. 1, curve 2) are considerably more active than the others [54]. So, all data presented bellow are related solely to these adsorbed oxygen species.

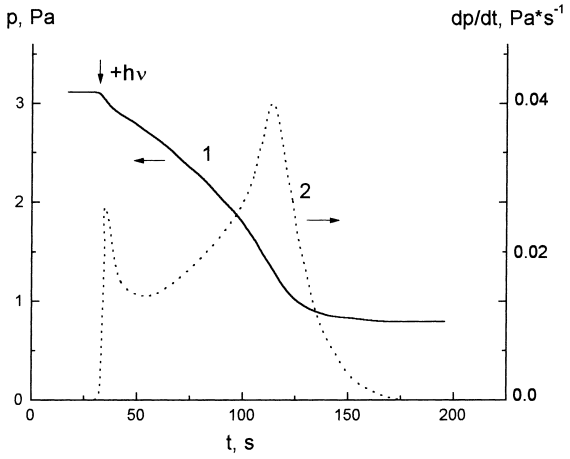

Fig. 4. Pressure dependence for O_2+H_2 mixture (curve 1) and the dependence of overall reaction rate (curve 2) on irradiation time during hydrogen photooxidation ($200<\lambda<250$ nm) over KBr vacuum deposited film. Initial pressure is $p_0(O_2)$=0.76 Pa and $p_0(H_2)$=2.3 Pa for oxygen and hydrogen, respectively. Arrows $\downarrow+h\nu$ point out the start of irradiation.

The steady-state initial reaction rate r_0 for the mechanism of H_2 photooxidation is

$$r_0 = -\frac{\mathrm{d}p(H_2)}{\mathrm{d}t} = \frac{k_a[O_2]_0 I k_r p_0(H_2)}{k_d + k_q p_0(O_2) + k_r p_0(H_2)} \qquad (8)$$

Here $[O_2]_0$ is the concentration of pre-adsorbed oxygen, I the light intensity, $p_0(H_2)$ and $p_0(O_2)$ are initial hydrogen and oxygen pressure.

The quenching of active adsorbed oxygen by gaseous oxygen is a significant feature of hydrogen photooxidation over KBr. In the case when H_2+O_2 gas mixture with the excess of hydrogen is admitted initially into reactor, quenching manifests itself as the acceleration of reaction with time (Fig. 4). The rate of H_2 consumption increases, and reaches maximum at the moment, when all gaseous oxygen is consumed. Note, that on H_2 photooxidation over KBr oxygen acts in another way if compared with organic molecules photooxidation in heterogeneous solvent/oxide systems [1]. On the other hand, the oxygen quenching during photooxidation over KBr follows to the classic Stern–Volmer dependence for photoluminescence and photochemical reaction ((8), see also [54]).

Kinetics studies on H_2 photooxidation allowed one to obtain the ratio of rate constants [54]. Assuming that k_r (Eq. (7d)) is equal to the collision constant (cross-section is taken as $\sigma=5\times10^{-16}$ cm^{-2}), reaction rate constants are estimated (Table 2). Comprising the ratio of rate constants obtained with that for different electronically excited states laying below 6 eV (available energy of photons in our studies) for oxygen atoms and molecules, one may assume molecular oxygen species (O_2* (ads)) (Eqs. (7a)–(7d)), corresponding to free $O_2(^1\Delta_2)$ oxygen to be preferable [54]. The similar mechanism of H_2 photooxidation on MgF_2 and alkali earth fluorides has been reported in [55], and estimates of rate constants close in order of magnitude to those for KBr were obtained. The corresponding rate constants for H_2 photooxidation over alkali earth fluorides are also presented in Table 2.

However, recent hydrogen photooxidation studies on KBr [56] demand the revision of the simple mechanism discussed above. “Crucial” dependencies of hydrogen photooxidation rates on light intensity are shown in Fig. 5. At a relatively high hydrogen pressure (curve 1) reaction rate is proportional to the light intensity according to Eq. (8). At low hydrogen pressure reaction rate dependence on the light intensity goes under linear one (curve 2). (Similar light intensity dependence of oxygen photoadsorption rate over ZrO_2 and the rate of phenol oxidation over TiO_2 have been found [21].) It means that decay constant k_d (8) is the

Table 2
The rate constants corresponding to the mechanism of hydrogen photooxidation (Eq. (7)) for KBr and alkali earth metal fluorides

Metal halide	$(k_d/k_r)10^2$ Pa	k_q/k_r	k_q[a] $\times10^{11}$ cm^3 s^{-1}	k_d[a] s^{-1}	τ_d ms
KBr	2.0±0.3	17±3	22±3.8	70±12	14±2.5
MgF_2	5.6±0.8	2.4±0.6	5.3±1.3	301±43	3.3±0.5
CaF_2	1.2±0.1	13±6	29±13	64±5	16±1
SrF_2	1.2±0.2	1.9±0.3	4.2±0.7	64±11	16±3
BaF_2	5.1±1.2	2.2±0.2	4.9±0.4	274±16	3.6±0.2

[a] The estimates of quenching constant k_q and decay constant $k_d=(\tau_d)^{-1}$ for active oxygen species O_2* are made, assuming that k_r is equal to the collision rate constant (2.2×10^{-11} cm^3 s^{-1}).

pseudo first-order constant, and it increases with the increasing light intensity. To describe this dependence of H_2 photooxidation rate on the light intensity (Fig. 5) one may suppose that O_2^- (ads) ions are the initial photoadsorbed oxygen species. Then active oxygen generation (stage 1, Eq. (7a)) may be presented as

$$O_2^-(\text{ads}) + h\nu \rightarrow O_2^*(\text{ads}) + e \qquad (9)$$

Note different electron excited states of molecular oxygen are known to form during O_2^- ions photoexcitation (photodetachment) [57]. Similarly to mechanism [21], additional decay channel for active oxygen species may be suggested

$$2a\ \ O_2^*(\text{ads}) + e \rightarrow O_2^{-*}(\text{ads}) \rightarrow O_2^-(\text{ads}) \qquad (k_{\text{rec}}) \qquad (10)$$

where O_2^{-*} (ads) is an analog of excited O_2^- ion introduced in alkali halides lattice [58], and e is free photoelectrons, generated mainly through the solid along with the oxygen photoionization (Eq. (9)). If so, their steady-state concentration (e) $\sim I\tau_e$ is proportional to the light intensity I and free electrons life time τ_e, determined by the several pathways of carries recombination in the solid. Thus, overall decay constant k_d (8) can be presented as a sum of true first order decay constant k'_d (Eq. (7b)) and pseudo first-order decay constant $k''_d \propto k_{\text{rec}} I\tau_e$ (Eq. (10)). From the kinetic point of view, the corrections (Eqs. (7a)–(7d)) are sufficient to explain qualitatively the observed dependencies of reaction rate on the light intensity (Fig. 5). Actually, the adsorbed oxygen formation and decay pathways on KBr are more complex. Thus, the photodesorption of oxygen, preliminary photoadsorbed on KBr illumination in extrinsic bands ($200 \leq \lambda \leq 250$) is in the same spectral region. In this case O_2 photodesorption rates are considerably lower than O_2 photodesorption rate, affected by excitations in KBr. Presumably, oxygen photodesorption can serve as the additional channel of active oxygen decay, since O_2 photodesorption is strongly suppressed in the hydrogen presence [56]. Same phenomenon is also true for hydrogen photooxidation over SrF_2 [56]. Several pathways of active oxygen species decay on photooxidation reaction may be the reason for no regular changing of the reaction rate constants on fluorides (Table 2). The studies of hydrogen photooxidation on KBr are in progress now. Regardless the hydrogen photooxidation mechanism revision that must be done, hydrogen photooxidation on KBr seems to be another example of heterogeneous photoreaction, in which the interdependence of rate of reaction on pressure (concentration) and on the light intensity appears [21]. The participation of reaction intermediates (O_2^* (ads) in our case) in recombination with photoinduced carriers is most probably a common reason for described reaction rate interdependence for ZrO_2, TiO_2 [21] and KBr.

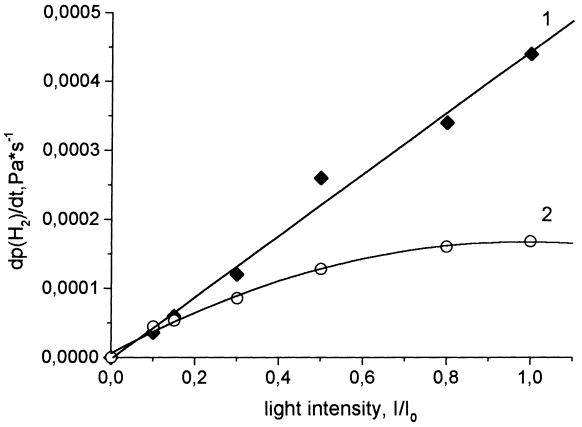

Fig. 5. The dependence of hydrogen photooxidation initial rate on the light intensity at initial hydrogen pressure $p_0(H_2)$=0.8 Pa (curve 1) and $p_0(H_2)$=0.04 Pa (curve 2). The highest light intensity (photon flux) is $I_0=2\times10^{15}$ photons $cm^{-2}\,s^{-1}$ ($200<\lambda<250$ nm). The amount of preliminary photoadsorbed oxygen taken in pressure units is 0.03 Pa.

For alkali metal iodides [17,54] and KBr [54] no photooxidation of H_2 and CO was observed under illumination in exciton absorption bands (λ=185 nm for KBr). Caused by excitons (Eq. (2)), a strong photostimulated desorption of oxygen, preliminary photoadsorbed under illumination in an extrinsic absorption bands ($200 \leq \lambda \leq 250$ for KBr), and generation of oxygen species inactive in relation to secondary photoexcitation suppress the photooxidation of small molecules in alkali halides exciton absorption bands.

3.5. Photodecomposition of carbon dioxide

Carbon dioxide photodecomposition (photolysis) was observed on 15 alkali halides tested [17]. The red limit of this reaction is estimated for KBr by $\lambda_r \approx 250$ nm [52]. On alkali halides illumination by mercury lamp of $\lambda \geq 200$ nm with CO_2 in the gas phase

CO_2 pressure decreases, evolving of CO evolves into the gas phase and oxygen accumulates at the alkali halides surface occurs. In contrast to O_2 and H_2, a strong adsorption of CO_2 in the dark is observed on most alkali halides. However, CO evolution into the gas phase is detected for KF, RbF and CsF only under illumination of samples with pre-adsorbed CO_2 and without carbon dioxide in the gas phase.

Fig. 6 illustrates some peculiarities of CO_2 photolysis over KBr under illumination in spectral range $\lambda \geq 200$ nm typical for most alkali halides, except for iodides. The kinetics of total gas pressure decreasing under illumination (Fig. 6, curve 1) is typical for photoadsorption. As total pressure decreases, partial CO pressure increases (curve 2). No oxygen is detected in the gas phase. With CO evolution into the gas phase, TPD shows that oxygen accumulates at the surface. Under continuous illumination both processes reach the saturation. Illumination drop changes nothing. CO_2 removal from the gas phase by it's low temperature condensation (the reactor is supplied by the special "finger", i.e., a tiny glass tube to condense CO_2 if needed) and repeated illumination cause the complete consumption of CO. After that only CO_2 is detected in the TPD spectra. "Finger" warming up completely restores reactor pressure before second illumination. However, after that solely CO_2 is registered in the reactor, both in the gas phase and on the sample surface. After that the cycle: illumination — condensation of CO_2 — repeated illumination — reinstitution of total CO_2 pressure can be reproduced 10 times without considerable changing of kinetics of CO evolution into the gas phase under the illumination. At this stage, in contrast to the very first illumination, no total pressure decrease is observed. Preliminary photoadsorbed oxygen does not influence the total pressure decrease (curve 3), but damps the CO evolution into the gas phase.

Obviously, three photoreactions do occur under KBr illumination (and most of alkali halides) provided that gaseous CO_2 (or $CO+O_2$) is in the system

$$\text{I. } CO_2(\text{gas}) + h\nu \rightarrow CO_2(\text{ads}) \quad (11)$$

$$\text{II. } CO_2(\text{gas}) + h\nu \rightarrow \tfrac{1}{2}O_2(\text{ads}) + CO(\text{gas}) \quad (12)$$

$$\text{III. } \tfrac{1}{2}O_2(\text{ads}) + CO(\text{gas}) + h\nu \rightarrow CO_2(\text{gas}) \quad (13)$$

Reaction I (Eq. (11)) is a non-dissociative and irreversible at room temperature carbon dioxide photoad-

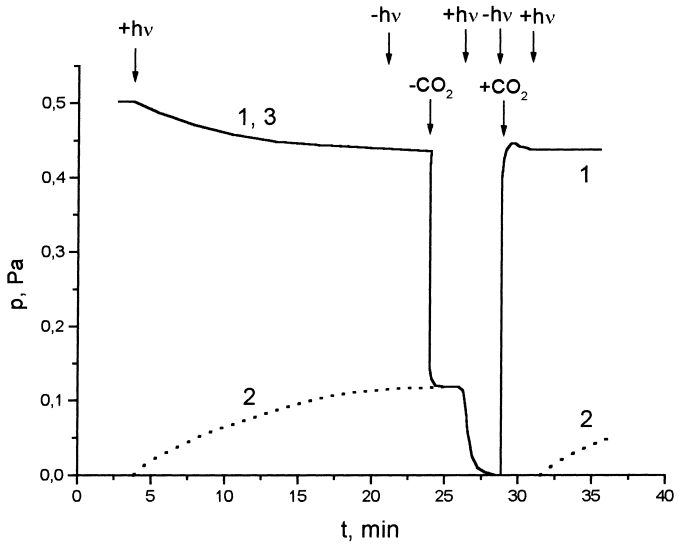

Fig. 6. The dependence of the overall pressure (curve 1) and the CO partial pressure (curve 2) on the irradiation time during CO_2 decomposition over KBr under illumination in spectral region $200 < \lambda < 250$ nm. The CO_2 pressure dependence on irradiation time with preliminary photoadsorbed ($200 < \lambda < 250$ nm, 0.5 Pa) oxygen (curve 3). Arrows $\downarrow + h\nu$ and $\downarrow - h\nu$ point out the switching on and switching out the light, respectively. Arrows $\downarrow - CO_2$ and $\downarrow + CO_2$ point out the removal and admittance of CO_2 into the gas phase.

sorption. It shows in the decrease of total and partial CO_2 pressure at the first illumination of alkali halides (Fig. 6, curve 1). The poorly resolved TPD spectra of photoadsorbed CO_2 were recorded for a few alkali halides at the background of a strong thermal desorption of CO_2 adsorbed in the dark. Surprisingly, but despite some similarity between the TPD spectra of photoadsorbed CO_2 and the TPD spectra of photoadsorbed O_2 no effect of pre-adsorbed oxygen on the non-dissociative CO_2 photoadsorption is found. So, one may assume that different surface centers are responsible for the photoadsorption of O_2 and CO_2 [53].

Along with reaction (I), dissociative photoadsorption (II) occurs (Eq. (12)). For example, the TPD spectrum of adsorbed oxygen recorded after a long time illumination of KBr with gaseous CO_2 in the reactor is presented in Fig. 1 (curve 4). The TPD spectrum of "photolytic" oxygen (curve 4) is not in full similar to that for oxygen photoadsorption (curve 2). Nevertheless, reaction (III), which is CO photooxidation, takes place, and process reaches the equilibrium. The equilibrium can be shifted towards photooxidation by adding photoadsorbed oxygen or by CO_2 removal from the gas phase as if it is thermal chemical equilibrium, which follows the Le Chatellier principle.

The activities of the alkali halides in the photodecomposition of CO_2, measured by the amount of CO (Δp), evolved into the gas phase for the 30 min irradiation at initial CO_2 pressure p=0.5 Pa are presented in Table 1. Note, that the average value of activity in the carbon dioxide photodecomposition for iodides (Δp_a=1.05 in the units of KBr activity) exceeds that for the rest alkali halides including fluorides (Δp_a=0.86). No correlation found between the CO_2 non-dissociative photoadsorption activities (PSA(CO_2)) with Δp(CO), accepted as the alkali halides activities in the CO_2 photolysis.

For alkali metal iodides and KBr under the illumination in exciton absorption bands the kinetics of CO_2 and CO pressure shows two distinct features. First, the non-dissociative CO_2 photoadsorption looks like "non-saturated" as in the case of oxygen photoadsorption [54]. Second, CO evolution rate into the gas phase does not reach saturation. CO evolution rate is practically constant provided that gaseous CO_2 remains in the reactor. The admittance of fresh portion of CO_2 into the reactor renews the reaction. Obviously, the latter feature is determined by the absence of CO photooxidation (Eq. (13)) under illumination of alkali halides in the exciton absorption bands. This peculiarity displays a sort of specific selectivity, named as the spectral selectivity of photocatalysts [16] which, in our case, is caused by the different adsorbed oxygen species forming under illumination of alkali halides in the different spectral regions. The possible reasons for the difference in the activity of adsorbed oxygen in the photooxidation of CO under irradiation in extrinsic and exciton absorption bands could be as follows: (i) excitons decay on structural mobile defects, specific for alkali halides crystals [8,9] can play some role in the formation of new type of surface active sites, which are not formed under excitation in an extrinsic absorption band, followed by oxygen adsorption yielding inactive oxygen species; (ii) oxygen photodesorption caused by photoinduced excitons removes the active forms of adsorbed oxygen from the surface. Thus, the ratio of active and inactive oxygen species on the surface depends on the wavelength of actinic light, and so does the selectivity of alkali halides catalysts towards either CO photooxidation or CO_2 photolysis.

The similar and even more impressive spectral selectivity of TiO_2 has been firstly reported by Kuzmin et al. [59]. In the case of methane conversion to ethane, ethylene and other hydrocarbons over TiO_2, the significantly higher chemical yield of hydrocarbons formation was observed on titania illumination in the extrinsic absorption region compared to that obtained under illumination in the fundamental absorption band, where the products of complete oxidation of methane dominate. With TiO_2, charge carriers (electrons and holes) are created under photoexcitation in both fundamental absorption band and extrinsic absorption region. In latter case the difference in the concentration of photoelectrons and photoholes at the surface, which depends on the wavelength of actinic light, can determine the spectral selectivity like described in [59]. The approach, based on the solution of continuity equation (Eq. (3)) which allows to consider semi-quantitatively the spectral selectivity determined by difference of concentration of photoholes and photoelectrons at the surface of solid catalysts, has been discussed elsewhere [21,50].

4. Conclusion

Several photostimulated reactions such as photoadsorption, photodesorption, photooxidation and photodecomposition of small molecules do occur at the surface of alkali halides. The pathways for the stimulation of surface reactions at alkali halides through the photogeneration of excitons and (or) free charge carriers in (i) fundamental absorption band; (ii) in extrinsic and intrinsic defect absorption bands and (iii) in UV-induced color centers bands are similar to those for the wide band-gap oxides. Alkali halides seem to be suitable model objects to study the mechanisms of photoexcitation of the wide band-gap solids resulting in the chemical transformations of molecules at their surface. On the other hand, the difference in the chemical structure of oxides and alkali halides makes the latter rather specific photocatalysts. Particularly, due to the absence of intrinsic oxygen in the alkali halides, they provide photoreactions (the photooxidation of H_2 and CO, the photodecomposition of CO_2), in which oxygen photoadsorption plays the significant role. In addition, the electronically excited adsorbed oxygen species are most probably the intermediates in the photooxidation reactions. The latter shows the resemblance between the mechanisms of heterogeneous photocatalytic and photochemical reactions.

Acknowledgements

I gratefully acknowledge stimulating and valuable discussions with Dr. I.S. Bobkova and Dr. A.V. Emeline.

References

[1] N. Serpone, E. Pelitzetti (Eds.), Photocatalysis — Fundamentals and Applications, Wiley/Interscience, New York, 1989.
[2] Yu.A. Gruzdkov, E.P. Savinov, V.N. Parmon, in: V.N. Parmon, K.I. Zamaraev (Eds.), Fotokataliticheskoe Preobrazovanie Solnechnoij Energii (Photocatalytic Conversion of Solar Energy), Nauka, Novosibirsk, 1991, p. 138.
[3] A. Mills, S. Le Hunte, J. Photochem. Photobiol. A 108 (1997) 1.
[4] J.H. De Boer, Zs. Phys. Chem. 21 (1933) 208.
[5] A.N. Terenin, Zurn. Fiz. Khim. 6 (1936) 189.
[6] Yu.P. Efimov, L.L. Basov, Yu.P. Solonitzyn, in: Th.I. Vilesov (Ed.), Uspekhi Fotoniki (Advances in Photonics), Vol. 4, LGU, Leningrad, 1974, p. 12.
[7] N.F. Mott, R.W. Gurney, Elektronnie processi v ionnich kristallach (Electronic Processes in Ionic Solids, Oxford 1948, translated in Russian). A.F. Joffe (Ed.), Foreign Literature Publishing House, Moscow, 1950, p. 304.
[8] Ch.B. Luschik, A.Ch. Luschik, Raspad Elektronnich Vozbuzdenii s Obrazovaniem Defectov v Tverdich Telach (The Decay of Electronic Excitations with Formation of Defects in Solids), Nauka, Novosibirsk, 1991.
[9] Defect and Impurity Centers in Ionic Solids. Optical and Magnetic Properties, Part 1 (special issue), J. Phys. Chem. Solids 51 (1990) 7.
[10] A.V. Aleksandrov, E.D. Aluker, I.A. Vasil'ev, A.F. Nechaev, S.A. Chernov, Vvedenie v Radiacionnuyu Fizikokhimiyu Poverchnosti Shelochno-Galoidnich Kristallov (Introduction in Radiation Physics and Chemistry of Alkali Halides Surface), Zinatne, Riga, 1989.
[11] M.A.A. Schoonen, Y. Xu, D.R. Strongin, J. Geochem. Explor. 62 (1998) 201.
[12] D.V. Pozdnjakov, V.N. Filimonov, K.Ya. Kondratjev, Dokl. Akad. Nauk USSR 235 (1980) 1097.
[13] V.S. Zakharenko, Catal. Today 39 (1997) 241.
[14] V.S. Zakharenko, V.N. Parmon, K.I. Zamaraev, Kinet. Katal. 38 (1997) 140.
[15] V. Isidorov, E. Klokova, V. Povarov, S. Kolkova, Catal. Today 39 (1997) 233.
[16] V.K. Ryabchuk, L.L. Basov, Yu.P. Solonitzyn, in: Th.I. Vilesov (Ed.), Uspekhi Fotoniki (Advances in Photonics), Vol. 7, LGU, Leningrad, 1980, p. 3.
[17] V.K. Ryabchuk, L.L. Basov, Yu.P. Solonitzyn, React. Kinet. Catal. Lett. 36 (1988) 19.
[18] V.K. Ryabchuk, L.L. Basov, Yu.P. Solonitzyn, Kinet. Katal. 19 (1978) 685.
[19] V.K. Ryabchuk, L.L. Basov, Yu.P. Solonitzyn, Khim. Fiz. 8 (1989) 1475.
[20] V.L. Rapoport, V.M. Antipenko, M.G. Malkin, Kinet. Katal. 9 (1968) 1306.
[21] A.V. Emeline, A.V. Rudakova, V.K. Ryabchuk, N. Serpone, J. Phys. Chem. B 102 (1998) 10906.
[22] G. Baldini, B. Bosacchi, Phys. Rev. 166 (1968) 863.
[23] I. Serna, L. Bru, Surf. Sci. 12 (1968) 369.
[24] A.M. Volodin, T.A. Bolshov, V.A. Konovalova, Mol. Eng. 4 (1994) 201.
[25] V.K. Ryabchuk, L.L. Basov, Yu.P. Solonitzyn, React. Kinet. Catal. Lett. 39 (1988) 331.
[26] V.K. Ryabchuk, G.V. Burukina, Zurn. Fiz. Khim. 65 (1991) 1621.
[27] Yu.P. Solonitzyn, Kinetika i Katakiz 7 (1968) 466.
[28] Yu.P. Solonitzyn, G.N. Kuzmin, A.L. Shurigin, V.N. Yurkin, Kinet. Katal. 15 (1974) 1580.
[29] A.V. Emelin, V.K. Ryabchuk, Russ. J. Phys. Chem. 71 (1997) 1881.
[30] S.V. Kurganov, Yu.M. Artem'ev, Vestnik LGU (St.-Petersburg State University) 4 (1988) 9.
[31] G.K. Wertheim, A. Hausman, W. Sander, The Electric Structure of Point Defects, North-Holland, Amsterdam, 1971.

[32] I.M. Prudnikov, private communication.
[33] E.Yu. Kotel'nikov, V.K. Ryabchuk, Vestnik SPESU (St. Petersburg State University), 2000, in press.
[34] E.D. Aluker, D.Yu. Lusis, S.A. Chernov, Elektronnie Vozbuzdeniia i Radioluminescencia Shelochno-Galoidnich Kristallov (Electronic Excitation and Radialuminescence of Alkali Halide Crystals), Zinatne, Riga, 1979.
[35] A.M. Stoneham, Theory of Defects in Solids, Part 2, Clarendon Press, Oxford, 1975.
[36] L. Apker, E. Taft, Phys. Rev. 107 (1951) 687.
[37] M.N. Lapushkin, N.S. Andreev, V.K. Ryabchuk, in: Yu.A. Zakharov (Ed.), Tezisi (Abstracts) III Vsesouyzn Konferencii po Radiacionnim Processam v Geterogennich Sistemach. Part.1, Kemerovo, 1982, p. 48.
[38] G.V. Burukina, G.E. Vitkovsky, V.K. Ryabchuk, Vestnik LGU (St.-Peterburg State University) 25 (1990) 93.
[39] A.V. Emeline, V.K. Ryabchuk, N. Serpone, J. Phys. Chem. B 102 (1999) 1316.
[40] E.B.D. Bourdon, I.P. Cowin, I. Harrison, I.C. Polanyi, C.D. Stanners, P.A. Young, J. Phys. Chem. 88 (1984) 6100.
[41] H.B. De Vore, Phys. Rev. 102 (1956) 86.
[42] S. Gristoloveanu, K.N. Kang, J. Phys. C 17 (1984) 699.
[43] Yu.K. Dolgikh, L.L. Basov, V.K. Ryabchuk, A.F. Simonenko, S.G. Grenishin, Kinet. Katal. 19 (1978) 556.
[44] Th.Th. Wolkenstein, I.V. Karpenko, J. Appl. Phys. Suppl. 133 (1962) 460.
[45] W.J. Albery, P.N. Bartlett, J. Elecrochem. Soc. 31 (1984) 315.
[46] J.S. Curran, D. Lamouche, J. Phys. Chem. 87 (1983) 5405.
[47] Yu.A. Gruzdkov, E.P. Savinov, V.N. Parmon, Khim. Fiz. 7 (1988) 44.
[48] D.B. Fitchen, W.B. Fowler, in: W.B. Fowler (Ed.), Physics of Color Centers, Academic Press, London, 1968, p. 626.
[49] V.B. Kazansky, Kinet. Katal. 19 (1978) 279.
[50] A.V. Emeline, E.V. Lobintseva, V.K. Ryabchuk, N. Serpone, J. Phys. Chem. B 103 (1999) 1325.
[51] A.V. Emeline, S.V. Petrova, V.K. Ryabchuk, N. Serpone, Chem. Mater. 10 (1988) 3484.
[52] A.V. Emelin, V.K. Ryabchuk, Zurn. Fiz. Khim. 72 (1998) 512.
[53] V.K. Ryabchuk, L.L. Basov, Yu.P. Solonitzyn, Kinet. Katal. 19 (1978) 928.
[54] Yu.P. Solonitzyn, L.L. Basov, V.K. Ryabchuk, Zurn. Fiz. Khim. 54 (1980) 2619.
[55] E.P. Mesheryakov, A.V. Emelin, V.K. Ryabchuk, T.S. Minakova, Russ. J. Kinet. Catal. 33 (1992) 469.
[56] A.V. Emeline, E.V. Lobintseva, A.V. Rudakova, V.K. Ryabchuk, Abstract, IPS-12, Berlin, Germany, August 1998, 3W93.
[57] L.C. Lee, G.P. Smith, J. Chem. Phys. 70 (1979) 1727.
[58] J. Rolfe, J. Chem. Phys. 70 (1979) 2463.
[59] G.N. Kuzmin, M.V. Knatko, S.V. Kurganov, Kinet. Catal. Lett. 23 (1983) 313.